Published in final edited form as:
Acta Biomater. 2010 July ; 6(7): 2467–2476. doi:10.1016/j.actbio.2010.02.002.

Mechanical and Microstructural Properties of Polycaprolactone Scaffolds with 1-D, 2-D, and 3-D Orthogonally Oriented Porous Architectures Produced by Selective Laser Sintering

Shaun Eshraghi and **Suman Das***
George W. Woodruff School of Mechanical Engineering, 801 Ferst Drive, Georgia Institute of Technology, Atlanta, GA 30332-0405, U.S.A.

INTRODUCTION

In the US, approximately 1.5 million surgical procedures are conducted annually to repair damaged or fractured bone [1]. Conventional treatments involve the use of autogenous bone-grafts or allogenic bone. However, the amount of donor tissue available and complications at the donor site are limiting factors for autogenous bone grafting. In the case of allogenic bone-grafts, cell-mediated immune responses and pathogen transfer can be problematic [2–4]. Tissue engineering has the potential to resolve these areas of concern. It holds great promise for providing improved patient care and decreased health care costs by reducing the number of surgical procedures and recovery time associated with current medical practices.

Tissue engineering focuses on the use of cells and engineered materials to restore tissue as opposed to making repairs using autografts, allografts, and prosthetics [5,6]. It has been observed that isolated cells are unable to form mechanically and physiologically suitable neotissues if growth is left unassisted [7]. Consequently, tissue engineering typically involves the use of porous, bioresorbable scaffolds to serve as temporary, three-dimensional scaffolds to guide cell attachment, differentiation, proliferation, and subsequent tissue regeneration. Recent research strongly suggests that the choice of scaffold material and its internal porous architecture significantly affect regenerate tissue type, structure, and function [8,9]. The effects of mean pore size has been extensively studied [8,10–16], and Chang et al showed that the direction of bone ingrowth was along the long axis of the porous channels [10]. In addition to possessing the appropriate material composition and internal pore architecture for regenerating a specific target tissue, scaffolds must also have mechanical properties appropriate to support the newly formed tissue [17,18]. In the case of bone, failure to provide adequate mechanical load-bearing function will cause a loss of function as the scaffold defines the ultimate shape of the new bone [18].

Conventional methods for scaffold fabrication rely on a variety of techniques involving the use of woven and non-woven fabrics, solvent casting and particulate leaching, solution casting and gel casting with porogens, pressurized gas foaming, forging, injection molding, cold or hot pressing, and electrospinning. However, these methods provide inadequate control over

*Corresponding author: sumandas@gatech.edu.

the porous architecture and require a separate mold for each exterior geometry [19]. An alternate approach known as direct digital manufacturing (DDM) combines the use of computer-aided design (CAD) and finite element analysis (FEA) techniques to design scaffolds with interior porous architectures that achieve the desired effective mechanical properties, and the use of solid freeform fabrication (SFF) methods to construct scaffolds that are reproducible, cost-effective, and consistent with these designs. SFF methods build three-dimensional objects layer-by-layer, depositing or consolidating materials in selected regions thereby enabling the rapid investigation of a wide range of scaffold geometries with a high degree of dimensional control and with fewer limitations on the scaffold exterior shape or the porous architecture. Consequently, scaffold fabrication through SFF has received worldwide attention. Extensive reviews on the emerging use of solid freeform fabrication and computer-aided design methods in tissue engineering are available in the literature [7,18–29].

Selective Laser Sintering (SLS) is a laser-based SFF technique in which an object is built layer-by-layer using powdered materials, radiant heaters, and a computer controlled laser [30]. In SLS, the digital representation of an object is mathematically sliced into a number of thin layers. The object is then created by scanning a laser beam and selectively fusing (melting or sintering) patterns into sequentially deposited layers of a powder. Each patterned layer of powder is also fused to its underlying layer and corresponds to a cross-section of the object as determined from the mathematical slicing operation. This layered manufacturing method allows the fabrication of scaffolds with a high degree of geometric complexity and enables the direct conversion of a scaffold's computer model into its physical realization—allowing patient-specific and tissue-specific reconstruction strategies to be easily developed [22,31–37]. In order to investigate the capabilities of a scaffold fabrication technique such as selective laser sintering in making functional scaffolds for load-bearing tissues, it is crucially important to assess the attainable mechanical properties both in bulk and in porous specimens, and to compare them against published data. SLS of non-resorbable materials has been investigated by several groups worldwide for biomedical applications such as tissue engineering and drug delivery [38–46]. More recently, the SLS has been used to fabricate tissue engineering scaffolds from bioresorbable polymeric biomaterials and their composites [47–58]. While these efforts have shown promise by documenting the feasibility of fusing powder particles together by laser sintering of such materials to form scaffold, they have not reported on the range of attainable mechanical properties when the designed solid regions, i.e. the struts of the scaffold, are fully or near-fully dense.

In a previous article [57], we demonstrated a bone tissue engineering approach using polycaprolactone scaffolds fabricated by SLS. The porosity of these scaffolds was between 37 and 55%, the compressive modulus of such scaffolds was in the 52–68MPa range, and the ultimate compressive strength was in the 2.0–3.2MPa range. Such scaffolds were shown to have ompressive mechanical properties within the reported lower range of properties for human trabecular bone. However, in that work, the scaffolds were shown to be incompletely dense in the designed solid regions resulting in approximately 20% porosity where none was intended. This porosity, termed manufacturing-induced porosity, results from the incomplete coalescence of polymer particles during sintering, melting and resolidification. Furthermore, the designed porosity composed of orthogonal porous channels, was not faithfully reproduced according to design due to excess powder being sintered and bonded to the pore channel interior surfaces, resulting in actual total porosity of the scaffold being less than the design porosity. Both of these effects were attributed to the use of sub-optimal SLS processing parameters, including the laser power, the scan speed, and the powder bed preheat temperature. Subsequently, we conducted a thorough study to identify optimal SLS processing parameters (Table 1) based on a design of experiments approach [58]. This study resulted in the development of processing parameters that achieved densities in excess of 95% relative density

in the designed solid regions of the scaffold while faithfully constructing the overall scaffold and the pore geometry to within 3–8% of designed dimensions.

This article reports on the tensile and compressive mechanical property testing, finite element analysis and microtomographic microstructure assessments carried out on PCL scaffolds produced by SLS using the improved processing parameters. To the best of our knowledge, this article represents the first effort to report both tensile and compressive mechanical properties of SLS-processed, solid PCL and porous PCL specimens using the same manufacturing technique, under identical conditions. The capability of producing anatomic shaped scaffolds with complex designed porous architecture and the potential of SLS as a versatile technique for fabricating functional bone tissue engineering scaffolds for load bearing applications can then be considered a direct extension of this work [57,58].

MATERIALS AND METHODS

Polycaprolactone powder properties

Test specimens were fabricated using polycaprolactone (PCL) powder marketed by Solvay Caprolactones (Warrington, UK) under the brand name CAPA® 6501 (Solvay Caprolactones has since been acquired by Perstorp, Sweden). PCL is a semicrystalline (56%) aliphatic thermoplastic having a melting point of 58–60°C and a glass transition temperature of approximately −60°C [59]. Gel Permeation Chromatography (GPC) analysis (THF, 25°C) was conducted to determine the molecular weight of CAPA® 6501 both before and after processing (pre-processed PCL: M_n = 91,900 ± 7,700; post-processed PCL: M_n = 73,000 ± 6,300). Mechanical test sieving conducted according to ISO 2591-1 standards confirmed that the powder has an average particle size of 90μm and a distribution in which 98% of all particles are less than 125μm in size (no particles > 150μm). The PCL powder was processed using a Sinterstation® 2000 commercial SLS machine (3D Systems Inc., Valencia, CA). Preheated and sequentially deposited powder layers were scanned using a low power continuous wave CO_2 laser (λ=10.6μm, power <10W) focused to a 450μm spot. Further details on SLS processing and process parameter selection are reported elsewhere [58].

Scaffold Design and Fabrication

Mechanical tensile and compressive test specimens were designed with solid and porous gage sections using UNIGRAPHICS™ software and exported to STL format. The solid tensile specimens conformed to the ASTM D638-03 specimen geometry whereas the compressive test specimens conformed to the ASTM D695-02a cylindrical geometry. Both tensile and compressive porous test specimens incorporated a network of 2mm × 2mm square channels in one, two and three-dimensions separated by 700μm struts yielding the corresponding 1-D, 2-D and 3-D porous specimens (henceforth referred to as D638-1D, D638-2D and D638-3D for the tensile specimens and D695-1D, D695-2D and D695-3D for the compressive specimens). The designed porosities for the tensile specimens were 56.87%, 67.4% and 83.3%, respectively, while the designed porosities for the compressive specimens were 51.1%, 68.5% and 80.90%.

The STL files were then used to fabricate the test specimens by SLS using CAPA® 6501 PCL powder in a Sinterstation™ 2000 machine. Solid specimens were built with the length of the specimens oriented either perpendicular or parallel to the build direction to investigate anisotropy in bulk material properties as a function of build orientation. The porous specimens were built with length oriented parallel to the build direction for the compressive specimens and perpendicular to the build direction for the tensile specimens because the bulk yield strength for the solid gage sections was highest in these manufacturing directions.

Mechanical Testing

Tensile and compressive testing was conducted in accordance with ASTM standards D638 Type 3 and D695 Type 2a respectively. Mechanical testing was conducted on SLS-processed PCL specimens both parallel and perpendicular to the SLS build direction (i.e. across and along direction of layer stacking). The schematic in Figure 1 illustrates the test geometries, dimensions, build orientations, and loading directions. Tensile specimens were tested using a displacement controlled Instron 4206 tensile testing machine (Instron Corp., Canton, MA) at a displacement rate of 50 mm/min. Each specimen was loaded to failure or until the maximum allowable crosshead travel (433mm) was reached. Compressive specimens were mechanically tested using a MTS Alliance RT30 test frame (MTS Systems Corp., Eden Prairie, MN). Specimens were compressed to 50% strain between two steel plates at a rate of 1 mm/min after an initial preload of 6.7 N (1.5 lb) was applied. The tensile and compressive properties reported for specimens incorporating porous gage sections correspond to effective values of stress and strain.

Finite Element Analysis

Stiffness constants for the porous scaffolds were calculated by using COMSOL Multiphysics (COMSOL Group, Stockholm, Sweden) and compared to the results from mechanical testing. The testing geometries in STL format were imported directly into the Structural Mechanics Module in COMSOL. Tensile geometries were modified by placing symmetry conditions about the y-z and z-x planes (z being the long axis of the scaffold) to reduce the number of elements. The models were meshed using 14575, 33573 and 93919 tetrahedral elements for D638-1D, D638-2D and D638-3D and 6818, 16510 and 46568 tetrahedral elements for D695-1D, D695-2D and D695-3D. Material properties were assumed homogenous and isotropic based on optical microscopy [58], mechanical testing (Table 2) and previous FEA on SLS processed PCL [51,57]. The Young's moduli (343.9MPa for tensile loading and 297.8MPa for compressive loading) used in the analysis were determined experimentally from the solid gage sections. The Poisson's ratio was assumed to be 0.3. The solution was found using a stationary solver at an axial strain of 0.01 in the z-direction.

Microstructural characterization by micro-computed tomography

One test specimen from each geometry type was scanned using a MS8X-130 Enhanced Vision Systems micro-computed tomography (μ-CT) machine (GE Medical Systems, Toronto, Canada) at a voxel resolution of 28.1μm. GEMS Microview software (GE Medical Systems, Toronto, Canada) was then used to determine the total (designed) porosity and the level of manufacturing induced porosity by selecting a region of interest (ROI) that encompassed the entire scaffold and then segmenting the processed PCL from air using an autothresholding procedure described previously [57].

RESULTS AND DISCUSSION

Scaffold Fabrication

SLS is a heat intensive manufacturing process and involves thermally induced densification of powder particles by sintering and/or melting. For any given material, the choice of SLS processing parameters will determine whether or not the material can be formed into structurally strong and dimensionally accurate shapes that faithfully render the corresponding digital design for that shape. Sub-optimal SLS processing parameters can lead to thermal growth and bonding of surrounding powder to a part's boundaries, dimensional inaccuracies and manufacturing induced porosity in the designed solid regions of a part due to incomplete densification of the powder particles, as was observed in our previous work [57]. In another study [58], a two-level factorial design of experiments (DOE) was conducted to analyze the

effects of five SLS processing parameters, namely, laser power, scan speed, scan spacing, part bed temperature, and powder layer delay time on resulting PCL part quality. The study demonstrated that parts fabricated at these settings were found to be easily removed from surrounding support powder, dimensionally accurate (to within 3–8% of design dimensions when measured using a Mitutoyo Digimatic Caliper with 0.01 mm resolution), and near-fully dense (>95%) as determined by planar area-based void fraction analysis of cross-sectional optical micrographs. The optimal parameters determined from that study were used to fabricate tensile and compressive mechanical specimens (Figure 2) with the highest level of densification in the designed solid regions while at the same time maximizing dimensional accuracy of the formed porous architecture.

Mechanical Properties

While the bulk tensile mechanical properties of PCL have been reported in the literature by manufacturers and researchers, we found no published data for the bulk compressive properties of PCL from manufacturers and only limited data on the bulk compressive mechanical properties of PCL from researchers. There does not appear to be one single comprehensive literature source that reports tensile and compressive properties of polycaprolactone for bulk or porous structures along with their relation to the molecular weight and manufacturing technique.

The manufacturer, Perstorp [59], of the PCL powder used in this study reported a tensile modulus of 430MPa at a strain rate of 10mm/min for injection molded CAPA 6500 (M_n= 47,500). Pitt et al. [60,61] extensively studied the degradation of PCL and reported a tensile modulus of 264.8MPa for melt extruded PCL capsules (M_n=50,900). Wehrenberg [62] reported a tensile strength of 19.3MPa and tensile modulus of 340MPa and Feng et al. [63] reported a tensile strength of 21.6MPa for compression molded specimens (M_n=45,000). Engelberg and Kohn [64] reported a tensile modulus of 400MPa and tensile strength of 16MPa for compression molded PCL (M_n=42,500) and also noted that solvent casting of PCL was not successful possibly due to its high crystallinity. Several other groups [65–68] have also reported the tensile mechanical properties of bulk PCL processed by conventional methods, and the values they reported can be found in Table 3.

The tensile mechanical property measurements for SLS-processed solid and porous PCL specimens with their long axis oriented both parallel (across layers) and perpendicular (along layers) to the build direction are listed in Table 2 along with manufacturer reported values for injection molded solid specimens. Even though the mechanical properties of SLS processed PCL exhibit slight dependence on the build orientation, they are comparable to those of PCL processed via injection molding. For bulk PCL, we found the mean tensile strength to be 16.1MPa in the perpendicular build orientation, the mean Young's modulus to be 343.9–363.4MPa depending upon the build orientation and the mean 0.2% offset yield strength to be 8.2–10.1MPa depending upon build orientation. Further, the strain at break was in excess of 790% for the perpendicular build orientation. We found that both the tensile strength and Young's modulus fall in the lower range of values reported in the literature. For the porous specimens, we found that the tensile strength and Young's modulus undergo a significant reduction relative to the bulk properties. For the D638-1D specimens, the mean tensile strength was 4.5MPa and the mean Young's modulus was 140.5MPa, indicating a reduction to approximately 28% and 40% of the respective bulk values. For D638-2D and D638-3D, the reduction in tensile properties was even more drastic, with the tensile strength and modulus of D638-2D reduced to 7.5% and 12% of the respective bulk values while the tensile strength and modulus of D638-3D were reduced to 7% and 10% respectively of the bulk values. It should be noted that the reduction in D638-3D (80.9% designed porosity) relative to D638-2D (68.5% designed porosity) was very small, as can be seen in Table 2 and Figure 3.

Compressive mechanical properties of PCL scaffolds manufactured through SFF have been previously reported in the literature by several groups. Zein et al. [69] have manufactured PCL scaffolds (M_n=87000) using fused deposition modeling (FDM) and reported mechanical properties ranging from a compressive modulus of 4MPa and a strength of 0.4MPa at 77% porosity to a compressive modulus of 77MPa and strength of 3.6MPa at 48% porosity. Recently, Shor et al. used precision extruding deposition (PED) to create PCL scaffolds with a compressive modulus of 59MPa and a strength of 5.3MPa at 65% porosity and solid gage specimens with a compressive modulus of 109MPa. Kim et al. [70], using a multi-headed deposition system (MHDS), produced PCL scaffolds (M_n=65000) with a compressive modulus of 21.4MPa and a strength of 1.3MPa at 69.6% porosity. Williams et al. [57] used an unoptimized SLS process to manufacture porous PCL scaffolds (M_n=50,000) with designed porosity between 37 and 55% with compressive moduli of 52–68MPa and compressive strengths of 2.0–3.2MPa. Recently, Cahill et al. [51] reported a compressive modulus of 47MPa for bulk PCL processed by SLS and 6MPa for PCL scaffolds at 55% porosity. Table 4 lists some of the compressive properties reported in the literature of PCL scaffolds manufactured through SFF.

The compressive mechanical properties of bulk and porous PCL specimens measured in this study are reported in Table 2. Reported here, for bulk PCL, the mean compressive modulus was 299–317.1MPa and the mean 0.2% offset yield strength was 10.3–12.5MPa depending on the build orientation. It should be noted that the compressive modulus reported here is over two times higher than that previously obtained using unoptimized SLS parameters [57]. As in the case of the tensile porous specimens, there was a drastic reduction in the compressive properties relative to the bulk. For D695-1D, yield strength and elastic modulus were reduced to 37% and 43% of the bulk values respectively. For D695-2D, the elastic modulus and yield strength were both reduced to approximately 4% of the respective bulk values; while for D695-3D, these values were reduced to 3.7% and 4.8% of the respective bulk values. Similarly to the tensile test specimens, the change in mechanical properties for D695-3D porous specimens (83.1% designed porosity) relative to D695-2D specimens (67.4% designed porosity) was very small.

To summarize, 1-D, 2-D and 3-D orthogonally porous PCL compressive specimens with 2mm × 2mm square pore channels and 700μm struts were produced by SLS, having a mean compressive modulus between 14.9 and 113.4MPa and an ultimate compressive strength between 0.6 and 10.0MPa for porosities ranging from 44.8–76.5%. The compressive mechanical properties presented here are the highest reported values for scaffolds produced by SLS and among the highest reported for similar scaffolds produced through other layered manufacturing techniques. The compressive modulus values of human trabecular bone range from 1 to 5000MPa and the ultimate compressive strength ranges from 0.1 to 27.3MPa [71–77] . Thus, the compressive mechanical properties of the porous PCL specimens reported in this work fall within the lower range of values reported for human trabecular bone.

Finite Element Analysis

Compressive and tensile effective moduli for the scaffold geometries predicted by FEA were in good agreement with the results from mechanical testing (Figure 3). The percent error for the FEA averaged 30%. The computational moduli reported here had better correlation with experimental moduli than was reported previously for SLS processed PCL by Williams et al. [57] who had a degree of underprediction averaging 100% using an image-based FEA technique, and recently by Cahill et al. [51] where the degree of overprediction was 67%. Since the bulk modulus used in the FEA was determined experimentally from solid gage specimens that have a higher average density than the scaffolds (Table 5), it was expected that the model would tend to over-predict the effective modulus of the scaffolds in all cases. However, the

FEA tended to underpredict the effective modulus of tensile specimens and overpredict the effective modulus of the compressive specimens.

The von Mises stress distributions in the tensile (Figure 4) and compressive (Figure 5) mechanical test specimens showed no elements above the respective bulk yield strengths at 1% strain. Observation of the stress distribution in both types of test specimens showed relatively low stress concentrations in the design solid regions that were changed to void regions in going from the 2-D to 3-D geometries, thus explaining the small change in mechanical properties between the 2-D and 3-D geometries.

Microtomographic microstructure

Figure 6 illustrates a representative volume-rendered μ-CT image of a porous compressive test specimen (D695-3D). Microstructural analysis of fully solid and porous cylindrical scaffolds processed by SLS (Table 5) showed that for fully solid specimens, the density ranged from 99.1% to 99.7% of full density, while for scaffolds with designed porous architecture, the density in the solid regions of the scaffold ranged from 92.7% to 98.6% of full density. While it should be noted that the μ-CT microstructural analysis could not detect any voids smaller than 28.1μm (the resolution of the μ-CT scanner), a majority of the manufacturing induced pores were >100μm in diameter as determined by cross-sectional optical microscopy.

CONCLUSIONS

We have demonstrated the capability of designing scaffolds endowed with 1-D, 2-D and 3-D orthogonally porous scaffolds for bone tissue engineering with desirable mechanical properties and then directly manufacturing them in PCL using SLS, a layered manufacturing technique. With the tensile and compressive mechanical properties of bulk PCL processed to near-full density through SLS serving as baseline mechanical properties for FEA, and the ability to process designed solid regions to near-full density in scaffolds while maintaining their dimensions accurate to within 3–8% of design dimensions, the agreement between experimentally measured and computationally modeled mechanical properties of our scaffold designs was excellent. This result establishes the basis for successfully achieving, via SLS, physical realizations of PCL scaffolds with targeted mechanical properties predicted through *a priori* FEA of the corresponding three-dimensional scaffold designs. Despite differences in exact composition and molecular weight, the tensile mechanical properties of solid PCL specimens, measured by us, compare well with several sources reported in the literature. The results of mechanical testing and FEA for both tensile and compressive properties showed a steep decline in mechanical properties as the degree of porosity increased. However, there was virtually no change in mechanical properties between 2-D to 3-D porous architectures. This is attributed to low stress concentrations in the design solid regions that were changed to void regions in going from the 2-D to 3-D design. The μ-CT image analysis of the PCL scaffolds confirmed the optical microscopy work in our previous study showing that the density in the designed solid regions was improved by the use of the new SLS processing parameters and this increase in density was correlated with improved mechanical properties.

Acknowledgments

This work was supported by the National Institute of Dental and Craniofacial Research (NIDCR) of the National Institutes of Health (NIH) under grant 5R21DE014736-02 and by the Georgia Institute of Technology.

REFERENCES

1. Einhorn TA. Clinical Applications of Recombinant Human BMPs: Early Experience and Future Development. J Bone Joint Surg Am 2003;85:82–88. [PubMed: 12925614]

2. Langer R. Tissue Engineering. Molecular Therapy 2000;1(1):12–15. [PubMed: 10933907]
3. Greenwald AS, et al. Bone-Graft Substitutes: Facts, Fictions, and Applications. J Bone Joint Surg Am 2001;83:S98–S103.
4. Laurencin CT, et al. Tissue Engineering: Orthopedic Applications. Annual Review of Biomedical Engineering 2003;1(1):19–46.
5. Langer R, Vacanti JP. Tissue engineering. Science 1993;260(5110):920–926. [PubMed: 8493529]
6. Griffith LG, Naughton G. Tissue Engineering--Current Challenges and Expanding Opportunities. Science 2002;295(5557):1009–1014. [PubMed: 11834815]
7. Yang S, Leong KF, Du Z, Chua CK. The design of scaffolds for use in tissue engineering. Part I. Traditional factors. Tissue Engineering 2001;7(6):679–689. [PubMed: 11749726]
8. Mikos AG, et al. Prevascularization of porous biodegradable polymers. Biotechnology and Bioengineering 1993;42(6):716–723. [PubMed: 18613104]
9. Bruder SP, et al. The Effect of Implants Loaded with Autologous Mesenchymal Stem Cells on the Healing of Canine Segmental Bone Defects. J Bone Joint Surg Am 1998;80(7):985–996. [PubMed: 9698003]
10. Chang B-S, et al. Osteoconduction at porous hydroxyapatite with various pore configurations. Biomaterials 2000;21(12):1291–1298. [PubMed: 10811311]
11. Karageorgiou V, Kaplan D. Porosity of 3D biomaterial scaffolds and osteogenesis. Biomaterials 2005;26(27):5474–5491. [PubMed: 15860204]
12. Murphy CM, Haugh MG, O'Brien FJ. The effect of mean pore size on cell attachment, proliferation and migration in collagen-glycosaminoglycan scaffolds for bone tissue engineering. Biomaterials. 2009 In Press, Corrected Proof.
13. Oh SH, et al. In vitro and in vivo characteristics of PCL scaffolds with pore size gradient fabricated by a centrifugation method. Biomaterials 2007;28(9):1664–1671. [PubMed: 17196648]
14. Zeltinger J, et al. Effect of Pore Size and Void Fraction on Cellular Adhesion, Proliferation, and Matrix Deposition. Tissue Engineering 2004;7(5):557–572. [PubMed: 11694190]
15. Goldstein AS, et al. Effect of Osteoblastic Culture Conditions on the Structure of Poly(DL-Lactic-co-Glycolic Acid) Foam Scaffolds. Tissue Engineering 1999;5(5):421–433. [PubMed: 10586098]
16. Mikos AG, et al. Preparation and characterization of poly(l-lactic acid) foams. Polymer 1994;35(5): 1068–1077.
17. Thomson R, et al. Biodegradable polymer scaffolds to regenerate organs, in Biopolymers II. 1995:245–274.
18. Hutmacher DW. Scaffolds in tissue engineering bone and cartilage. Biomaterials 2000;21(24):2529–2543. [PubMed: 11071603]
19. Hutmacher DW. Scaffold design and fabrication technologies for engineering tissues state of the art and future perspectives. Journal of Biomaterials Science, Polymer Edition 2001;12:107–124. [PubMed: 11334185]
20. Yang S, Leong KF, Du Z, Chua CK. The design of scaffolds for use in tissue engineering. Part II. Rapid prototyping techniques. Tissue Engineering 2002;8(1):1–11. [PubMed: 11886649]
21. Sachlos E, Czernuszka JT. Making tissue engineering scaffolds work. Review: the application of solid freeform fabrication technology to the production of tissue engineering scaffolds. European Cells Materials 2003;5:29–40. [PubMed: 14562270]
22. Hutmacher DW, Sittinger M, Risbud MV. Scaffold-based tissue engineering: rationale for computer-aided design and solid free-form fabrication systems. Trends in Biotechnology 2004;22(7):354–362. [PubMed: 15245908]
23. Sun W, et al. Computer-aided tissue engineering: overview, scope and challenges. Biotechnology and Applied Biochemistry 2004;39(Pt 1):29–47. [PubMed: 14563211]
24. Sun W, et al. Computer-aided tissue engineering: application to biomimetic modelling and design of tissue scaffolds. Biotechnology and Applied Biochemistry 2004;39(Pt 1):49–58. [PubMed: 14556653]
25. Weigel T, Schinkel G, Lendlein A. Design and preparation of polymeric scaffolds for tissue engineering. Expert Review of Medical Devices 2006;3(6):835–851. [PubMed: 17280547]

26. Seunarine K, et al. 3D polymer scaffolds for tissue engineering. Nanomedicine 2006;1:281–296. [PubMed: 17716159]
27. Salgado AJ, Coutinho OP, Reis RL. Bone Tissue Engineering: State of the Art and Future Trends. Macromolecular Bioscience 2004;4(8):743–765. [PubMed: 15468269]
28. Bártolo PJ, et al. Advanced Processes to Fabricate Scaffolds for Tissue Engineering, in Virtual Prototyping & Bio Manufacturing in Medical Applications. 2008:149–170.
29. Leong KF, Cheah CM, Chua CK. Solid freeform fabrication of three-dimensional scaffolds for engineering replacement tissues and organs. Biomaterials 2003;24(13):2363–2378. [PubMed: 12699674]
30. Deckard, CR. Selective Laser Sintering, in Mechanical Engineering. Austin: University of Texas at Austin; 1988.
31. Cesarano J III, et al. Customization of Load-Bearing Hydroxyapatite Lattice Scaffolds. International Journal of Applied Ceramic Technology 2005;2(3):212–220.
32. Dyson JA, et al. Development of Custom-Built Bone Scaffolds Using Mesenchymal Stem Cells and Apatite-Wollastonite Glass-Ceramics. Tissue Engineering 2007;13(12):2891–2901. [PubMed: 17764401]
33. Jiankang H, et al. Custom fabrication of composite tibial hemi-knee joint combining CAD/CAE/CAM techniques. Proceedings of the Institution of Mechanical Engineers, Part H: Journal of Engineering in Medicine 2006;220(8):823–830.
34. Moroni L, et al. Finite Element Analysis of Meniscal Anatomical 3D Scaffolds: Implications for Tissue Engineering. 2007
35. Popov VK, et al. Laser technologies for fabricating individual implants and matrices for tissue engineering. J. Opt. Technol 2007;74(9):636–640.
36. Saijo H, et al. Maxillofacial reconstruction using custom-made artificial bones fabricated by inkjet printing technology. Journal of Artificial Organs 2009;12(3):200–205. [PubMed: 19894095]
37. Wu G, et al. Selective laser sintering technology for customized fabrication of facial prostheses. The Journal of Prosthetic Dentistry 2008;100(1):56–60. [PubMed: 18589076]
38. Das S, et al. Freeform fabrication of Nylon-6 tissue engineering scaffolds. Rapid Prototyping Journal 2004;9(1):43–49.
39. Berry E, et al. Preliminary experience with medical applications of rapid prototyping by selective laser sintering. Medical engineering & physics 1997;19(1):90–96. [PubMed: 9140877]
40. Rimell JT, Marquis PM. Selective laser sintering of ultra high molecular weight polyethylene for clinical applications. Journal of Biomedical Materials Research 2000;53(4):414–420. [PubMed: 10898883]
41. Shishkovsky I, et al. The synthesis of a biocomposite based on nickel titanium and hydroxyapatite under selective laser sintering conditions. Technical Physics Letters 2001;27(3):211–213.
42. Tan K, et al. Fabrication and characterization of three-dimensional poly(ether-ether-ketone)/−hydroxyapatite biocomposite scaffolds using laser sintering. Proceedings of the Institution of Mechanical Engineers, Part H: Journal of Engineering in Medicine 2005;219(3):183–194.
43. Tan KH, et al. Scaffold development using selective laser sintering of polyetheretherketone-hydroxyapatite biocomposite blends. Biomaterials 2003;24(18):3115–3123. [PubMed: 12895584]
44. Cheah C, et al. Characterization of microfeatures in selective laser sintered drug delivery devices. Proceedings of the Institution of Mechanical Engineers, Part H: Journal of Engineering in Medicine 2002;216(6):369–383.
45. Leong K, et al. Fabrication of porous polymeric matrix drug delivery devices using the selective laser sintering technique. Proceedings of the Institution of Mechanical Engineers, Part H: Journal of Engineering in Medicine 2001;215(2):191–192.
46. Low KH, et al. Characterization of SLS parts for drug delivery devices. Rapid Prototyping Journal 2001;7(5):262–267.
47. Tan KH, et al. Selective laser sintering of biocompatible polymers for applications in tissue engineering. Bio-Medical Materials and Engineering 2005;15(1):113–124. [PubMed: 15623935]

48. Chua CK, et al. Development of tissue scaffolds using selective laser sintering of polyvinyl alcohol/hydroxyapatite biocomposite for craniofacial and joint defects. Journal of Materials Science: Materials in Medicine 2004;15(10):1113–1121. [PubMed: 15516872]
49. Wiria FE, et al. Poly-ε-caprolactone/hydroxyapatite for tissue engineering scaffold fabrication via selective laser sintering. Acta Biomaterialia 2007;3(1):1–12. [PubMed: 17055789]
50. Zhang H, Lin C-Y, Hollister SJ. The interaction between bone marrow stromal cells and RGD-modified three-dimensional porous polycaprolactone scaffolds. Biomaterials 2009;30(25):4063–4069. [PubMed: 19487019]
51. Cahill S, Lohfeld S, McHugh P. Finite element predictions compared to experimental results for the effective modulus of bone tissue engineering scaffolds fabricated by selective laser sintering. Journal of Materials Science: Materials in Medicine 2009;20(6):1255–1262. [PubMed: 19199109]
52. Ciardelli G, et al. Blends of poly-(ε-caprolactone) and polysaccharides in tissue engineering applications. Biomacromolecules 2005;6(4):1961–1976. [PubMed: 16004434]
53. Huang H, et al. Avidin-biotin binding-based cell seeding and perfusion culture of liver-derived cells in a porous scaffold with a three-dimensional interconnected flow-channel network. Biomaterials 2007;28(26):3815–3823. [PubMed: 17544499]
54. Kanczler JM, et al. Biocompatibility and osteogenic potential of human fetal femur-derived cells on surface selective laser sintered scaffolds. Acta Biomaterialia 2009;5(6):2063–2071. [PubMed: 19362063]
55. Lin L, et al. The Mechanical Properties of Bone Tissue Engineering Scaffold Fabricating Via Selective Laser Sintering, in Life System Modeling and Simulation. 2007:146–152.
56. Eosoly S, et al. Selective laser sintering of hydroxyapatite/poly-ε-caprolactone scaffolds. Acta Biomaterialia. In Press, Corrected Proof.
57. Williams JM, et al. Bone tissue engineering using polycaprolactone scaffolds fabricated via selective laser sintering. Biomaterials 2005;26(23):4817–4827. [PubMed: 15763261]
58. Partee B, Hollister SJ, Das S. Selective laser sintering process optimization for layered manufacturing of CAPA® 6501 polycaprolactone bone tissue engineering scaffolds. Journal of Manufacturing Science and Engineering, Transactions of the ASME 2006;128(2):531–540.
59. Biodegradable CAPA Thermoplastics. 2003
60. Pitt CG, et al. Aliphatic polyesters. I. The degradation of poly (ε-caprolactone) in vivo. J Appl Polym Sci 1981;26:3779–3787.
61. Pitt CG, et al. Aliphatic polyesters II. The degradation of poly (DL-lactide), poly (ε-caprolactone), and their copolymers in vivo. Biomaterials 1981;2(4):215–220. [PubMed: 7326315]
62. Wehrenberg RH. Lactic acid polymers: strong, degradable thermoplastics. Mater. Eng 1981;94(3):63–66.
63. Feng X, Song C, Chen W. Synthesis and evaluation of biodegradable block copolymers of ε-caprolactone and D,L-lactide. J. Polym. Sci. Polym. Lett 1983;21(8):593–600.
64. Engelberg I, Kohn J. Physico-mechanical properties of degradable polymers used in medical applications: A comparative study. Biomaterials 1991;12(3):292–304. [PubMed: 1649646]
65. Vandamme TF, Legras R. Physico-mechanical properties of poly(ε-caprolactone)for the construction of rumino-reticulum devices for grazing animals. Biomaterials 1995;16(18):1395–1400. [PubMed: 8590766]
66. Rosa DS, et al. Evaluation of the thermal and mechanical properties of poly(ϵ-caprolactone), low-density polyethylene, and their blends. Journal of Applied Polymer Science 2004;91(6):3909–3914.
67. Correlo VM, et al. Properties of melt processed chitosan and aliphatic polyester blends. Materials Science & Engineering: A 2005;403:57–68.
68. Granado A, Eguiazábal JI, Nazábal J. Structure and mechanical properties of blends of poly(ε-caprolactone) with a poly(amino ether). Journal of Applied Polymer Science 2008;109(6):3892–3899.
69. Zein I, et al. Fused deposition modeling of novel scaffold architectures for tissue engineering applications. Biomaterials 2002;23(4):1169–1185. [PubMed: 11791921]

70. Kim J, et al. Cell adhesion and proliferation evaluation of SFF-based biodegradable scaffolds fabricated using multi-head deposition system. Biofabrication 2009;1(1):5002.
71. Goldstein SA. The mechanical properties of trabecular bone: Dependence on anatomic location and function. Journal of Biomechanics 1987;20(11–12):1055–1061. [PubMed: 3323197]
72. Goulet RW, et al. The relationship between the structural and orthogonal compressive properties of trabecular bone. Journal of Biomechanics 1994;27(4):375–377. 379–389. [PubMed: 8188719]
73. Lang S, et al. Correlation of mechanical properties of vertebral trabecular bone with equivalent mineral density as measured by computed tomography. J Bone Joint Surg Am 1988;70(10):1531–1538. [PubMed: 3198678]
74. Lotz JC, Gerhart TN, Hayes WC. Mechanical Properties of Trabecular Bone from the Proximal Femur: A Quantitative CT Study. Journal of Computer Assisted Tomography 1990;14(1):107–114. [PubMed: 2298972]
75. Mow, V., et al. Basic orthopaedic biomechanics. Philadelphia: Lippincott-Raven; 1997.
76. Ouyang J, et al. Biomechanical characteristics of human trabecular bone. Clinical Biomechanics 1997;12(7–8):522–524. [PubMed: 11415763]
77. Porter BD, et al. Mechanical Properties of a Biodegradable Bone Regeneration Scaffold. Journal of Biomechanical Engineering 2000;122(3):286–288. [PubMed: 10923298]
78. Correlo VM, Boesel LucianoF, Bhattacharya Mrinal, Mano JoaoF, Neves NunoM, Reis RuisL. Hydroxyapatite Reinforced Chitosan and Polyester Blends for Biomedical Applications. Macromolecular Materials and Engineering 2005;290(12):1157–1165.
79. Hutmacher DW, et al. Mechanical properties and cell cultural response of polycaprolactone scaffolds designed and fabricated via fused deposition modeling. Journal of Biomedical Materials Research 2001;55(2):203–216. [PubMed: 11255172]
80. Lam CXF, Teoh SH, Hutmacher DW. Comparison of the degradation of polycaprolactone and polycaprolactone-(β-tricalcium phosphate) scaffolds in alkaline medium. Polymer International 2007;56(6):718–728.
81. Zhou Y, et al. In vitro bone engineering based on polycaprolactone and polycaprolactone-tricalcium phosphate composites. Polymer International 2007;56(3):333–342.
82. Wang F, et al. Precision extruding deposition and characterization of cellular poly-e-caprolactone tissue scaffolds. Rapid Prototyping Journal 2004;10(1):42–49.
83. Shor L, et al. Precision extruding deposition (PED) fabrication of polycaprolactone (PCL) scaffolds for bone tissue engineering. Biofabrication 2009;1(1):5003.

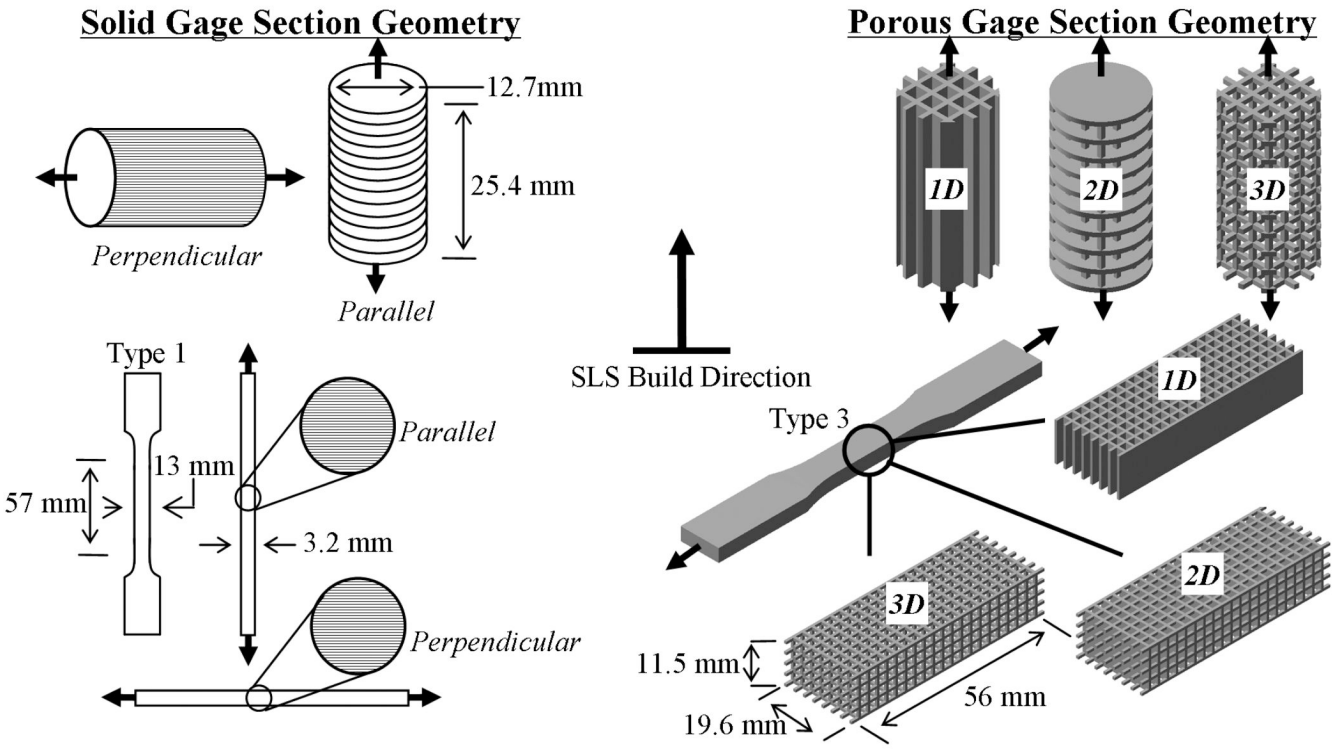

Figure 1.
Mechanical test specimen geometries, dimensions, build orientations, and loading directions.

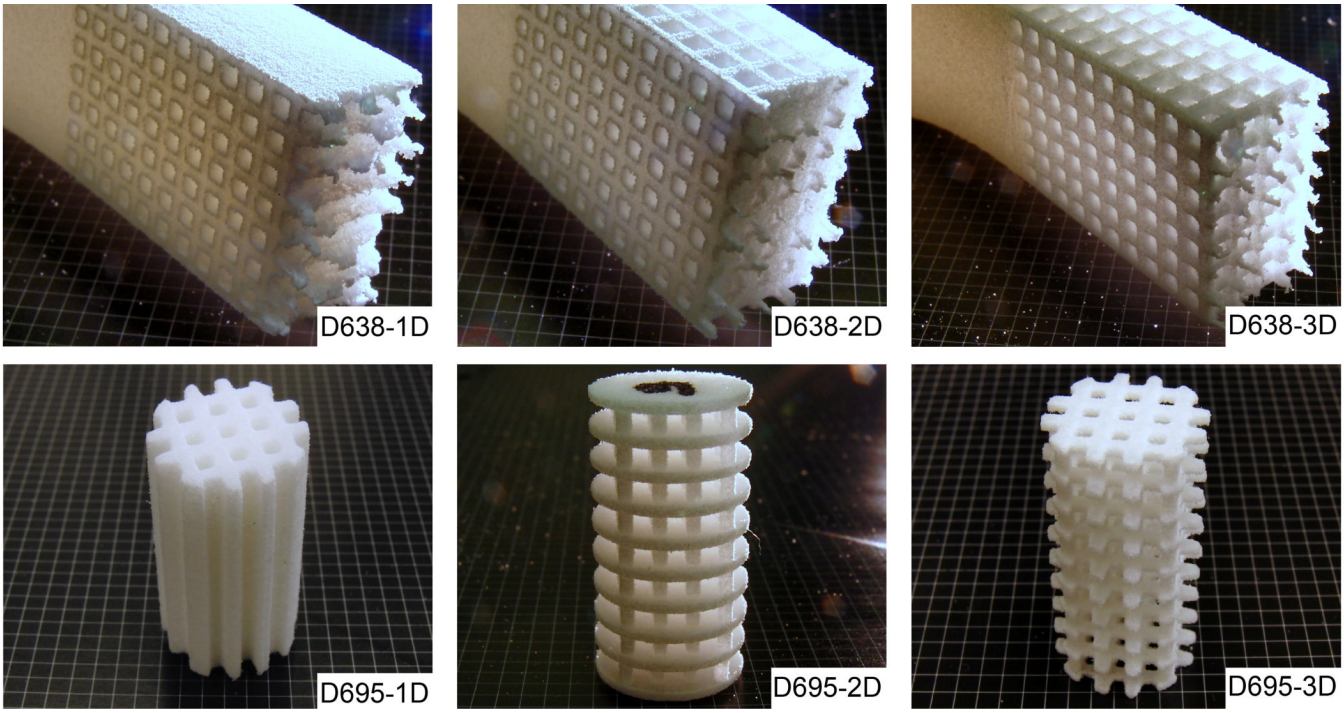

Figure 2.
SLS processed PCL tensile (D638-1D, D638-2D, and D638-3D) specimens (post-fracture) and compressive (D695-1D, D695-2D, and D695-3D) specimens with 1D, 2D and 3D orthogonal porous channels (placed on a 2mm grid).

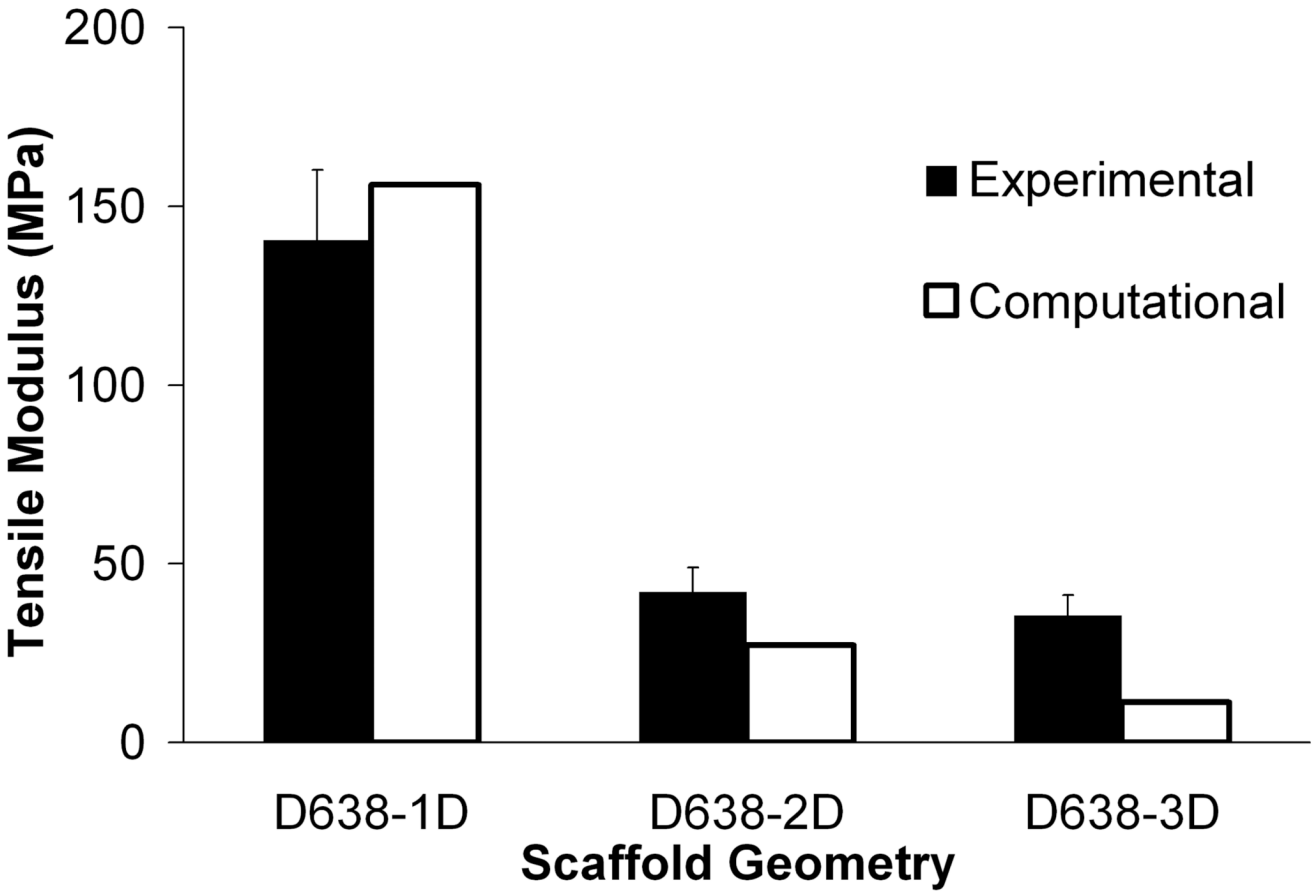

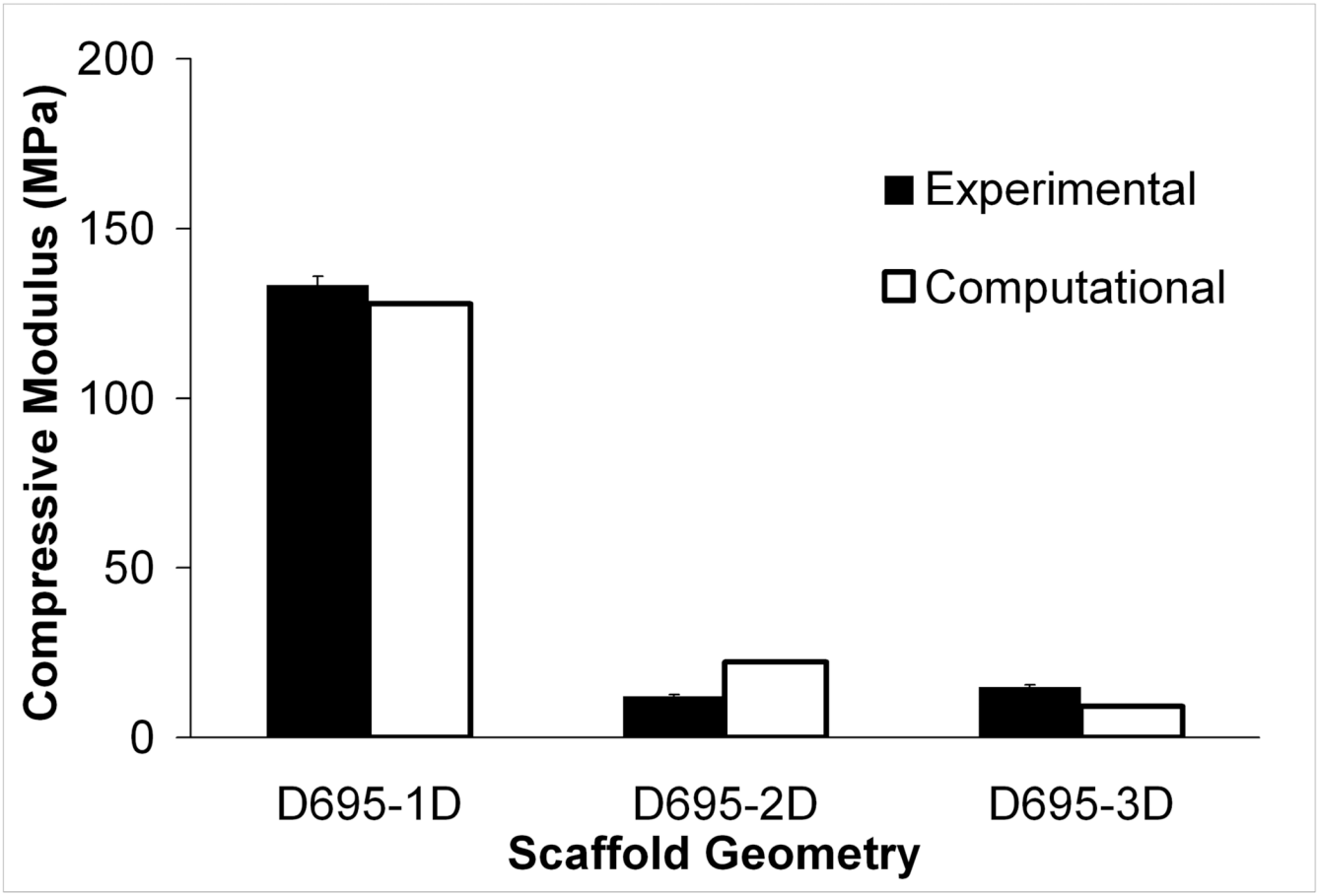

Figure 3.
Experimental and computational effective moduli for (a) tensile and (b) compressive specimens. Error bars denote standard devation (n=6).

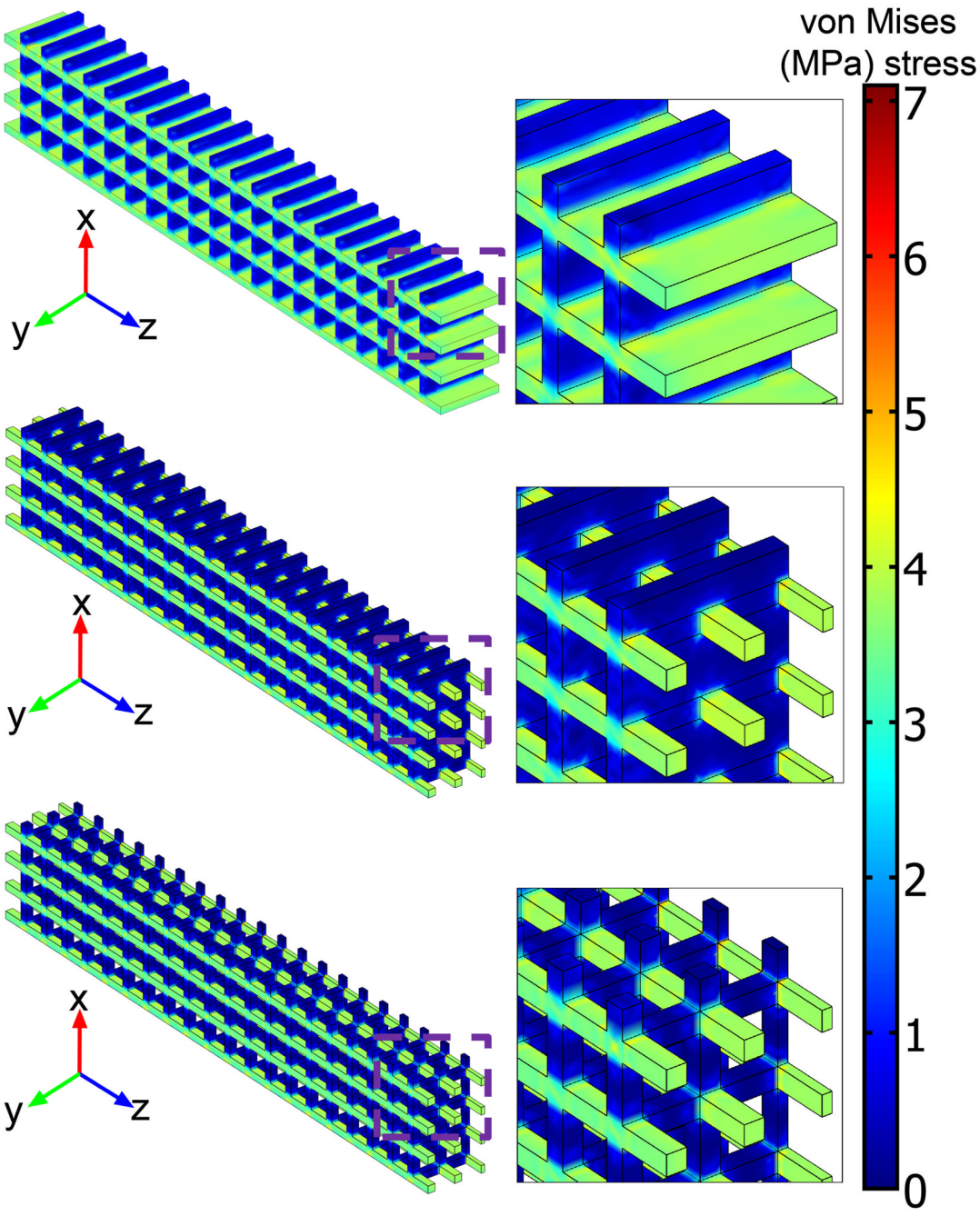

Figure 4.
Subdomain plots of von Mises stress distribution for porous tensile test specimens.

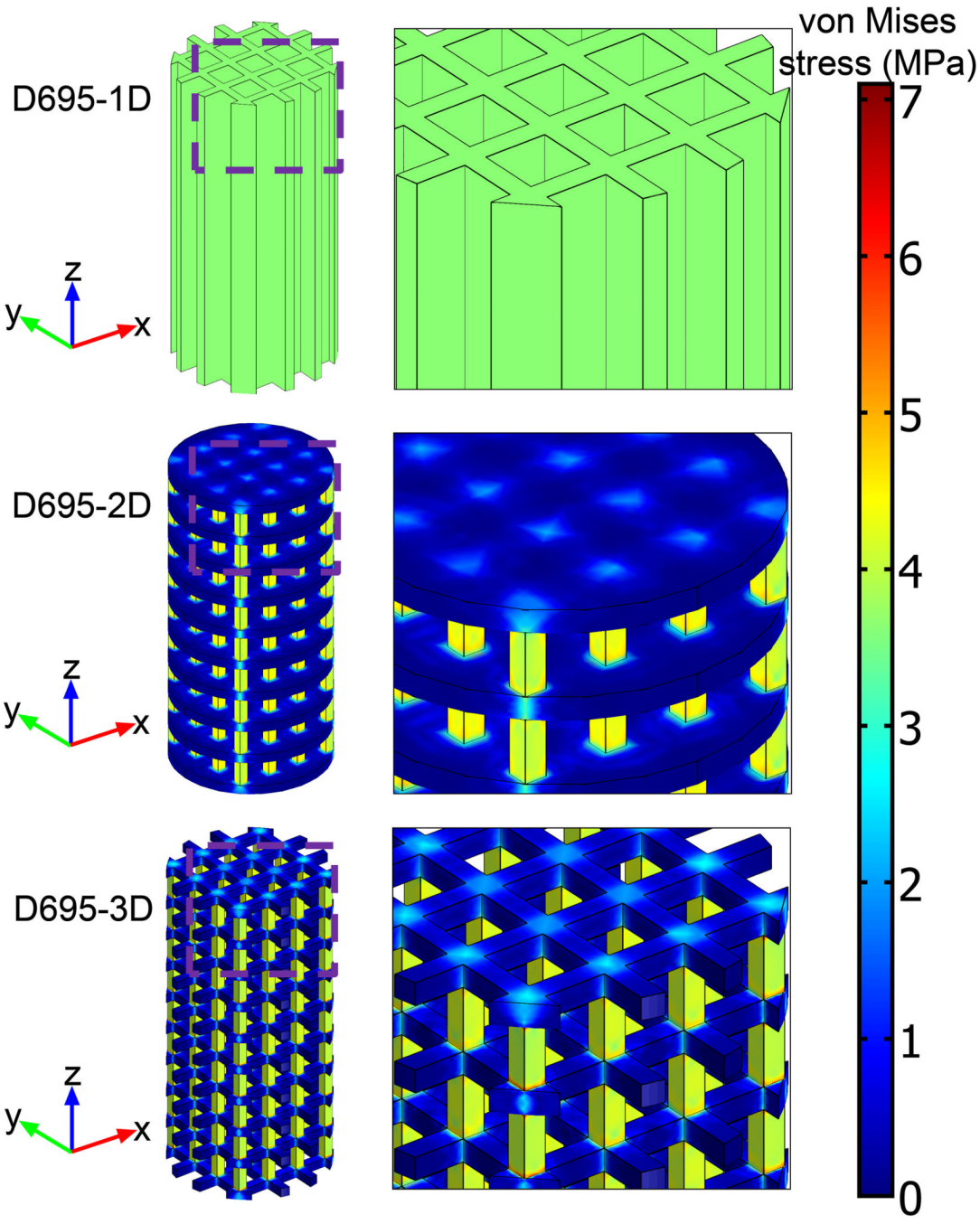

Figure 5.
Subdomain plots of von Mises stress distribution for porous compressive test specimens.

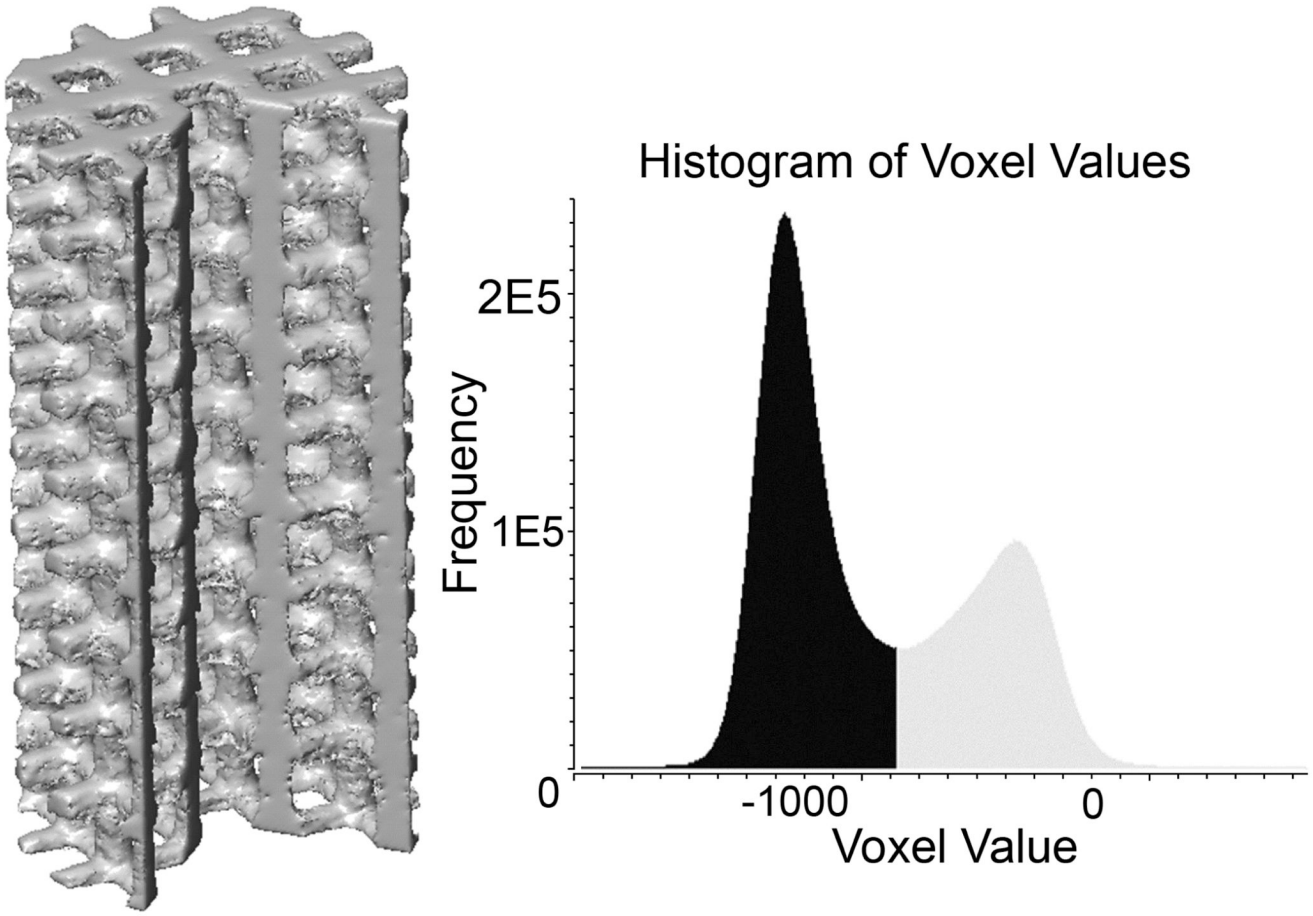

Figure 6.
μ-CT volume-rendered compressive test specimen along with voxel intensity histogram showing the threshold used to segment PCL (black) from air (grey).

Table 1

Optimal SLS parameter settings for processing PCL as determined by Partee et al [58].

Parameter	Setting	
	Solid	Scaffold
Laser power	4.1 W	4.1 W
Scan speed	1079.5 mm/sec	1079.5 mm/sec
Scan spacing	152.4 μm	152.4 μm
Part bed temperature	46°C	46°C
Powder layer delay	0 sec	8 sec

Table 2

Mechanical property assessment of bulk and porous SLS processed PCL.

	Property	Unit	SLS					Injection Molding[2]
			Solid Gage Section		Porous Gage Section[1]			
			//	⊥	1D	2D	3D	
Tension	Elastic Modulus, E	MPa	363.4 ± 71.6	343.9 ± 33.2	140.5 ± 19.6	42.0 ± 6.9	35.5 ± 5.8	430
	0.2% Offset Yield Strength, σ_Y	MPa	8.2 ± 1.0	10.1 ± 1.5	3.2 ± 0.6	0.67 ± 0.08	0.67 ± 0.06	17.5
	Strain at Yield, ε_Y	mm/mm	0.024 ± 0.006	0.031 ± 0.002	0.024 ± 0.001	0.017 ± 0.002	0.020 ± 0.002	---
	Ultimate Tensile Strength, σ_{UT}	MPa	10.5 ± 0.3	16.1 ± 0.3	4.5 ± 0.4	1.2 ± 0.2	1.1 ± 0.1	--
	Strain at Break, ε_B	mm/mm	0.043 ± 0.007	8.0 ± 0.3	0.095 ± 0.022	0.092 ± 0.022	0.096 ± 0.025	> 7
Compression	Elastic Modulus, E	MPa	297.8 ± 7.1	317.1 ± 3.9	133.4 ± 2.6	12.1 ± 0.5	14.9 ± 0.6	---
	0.2% Offset Yield Strength, σ_Y	MPa	12.5 ± 0.3	10.3 ± 0.2	4.25 ± 0.05	0.45 ± 0.01	0.42 ± 0.03	---
	Strain at Yield, ε_Y	mm/mm	0.052 ± 0.003	0.037 ± 0.002	0.0370 ± 0.000	0.0376 ± 0.001	0.0268 ± 0.003	---
	Ultimate Compressive Strength	MPa	38.7 ± 0.3	38.80 ± 0.66	10.0 ± 0.62	0.60 ± 0.00	0.60 ± 0.00	

Note: $\mu \pm \sigma$ where μ denotes the mean and σ denotes the standard deviation (n=6).

[1] Porous compressive specimens tested parallel to SLS build direction, porous tensile specimens tested perpendicular to SLS build direction.

[2] Reported by Perstorp Caprolactone, tests were conducted at a strain rate of 10mm/min to determine E and 100mm/min in all other cases.

Table 3

Bulk tensile mechanical properties of PCL reported in the literature.

Reference	Manufacturing Method	Tensile Modulus (MPa)	Tensile Strength (MPa)	Weight Average Molecular Weight, M_n	Number Average Molecular Weight, M_w
Perstorp [59]	Injection Molding	430		47500	84500
Pitt et al [60]	Melt Extruding	264.8		50900	84500
Wehrenberg [62]	Compression Molding	340	19.3		
Feng et al [63]	Compression Molding		21.6	45000	50400
Engelberg [64]	Compression Molding	400	16	42500	72500
Vandamme and Legras[65]	Compression Molding	251.9	N/A	50500	101000
Rosa et al [66]	Compression Molding	429.1	16.9	50000	80000
Corello [78]	Injection Molding	378	27.3	64,000	124,000
Granado [68]	Injection Molding	300	14		80,000

Table 4

Compressive mechanical properties of PCL scaffolds manufactured through SFF.

Reference	Manufacturing Method	Compressive Modulus (MPa)	Compresive Strength (MPa)	Porosity (%)	Weight Average Molecular Weight, M_n	Number Average Molecular Weight, M_w
Hutmacher [79]	FDM	41.9	3.1[a]	61	87343	146739
Zein [69]	FDM	4–77	0.4–3.6	48–77	87000	147700
Lam [80]	FDM	2.41	0.74	68	92000	140000
Zhou [81]	FDM	4.8	2.2	65		
Wang [82]	PED	150–200		53.1		44000
Shor [83]	PED	59	5.3	65		
Shor [83]	PED	109		0		
Kim [70]	PED	21.0	1.3	69.6	65000	
Williams [57]	SLS	52–68	2.0–3.2	37–55	50000	

[a] 0.1% offset yield

Table 5

Porosity of solid and porous scaffolds measured through μ-CT.

	ASTM Specimen	Designed Porosity (%)			Manufacturing Induced Porosity (%)	% of Fully Dense
		Measured[1]	Target[2]	Diff		
Solid	D638 //	Not Applicable			0.3	99.7
	D638 ⊥				0.9	99.1
	D695 //				0.4	99.6
	D695 ⊥				0.4	99.6
Porous	D638 1D	44.1	51.1	7.0	4.8	95.2
	D638 2D	57.5	68.5	11.0	2.6	97.4
	D638 3D	77.3	80.9	3.6	1.4	98.6
	D695 1D	44.8	56.9	12.1	2.9	97.1
	D695 2D	61.9	67.4	5.5	7.3	92.7
	D695 3D	76.5	83.3	6.8	3.4	96.6

[1] Calculated using GEMS Microview

[2] Calculated using Unigraphics